



## Registration of proton induced spallation products of U, Pb and Au in mica track detectors

S.R. Hashemi-Nezhad<sup>a,\*</sup>, I. Zhuk<sup>b</sup>, A. Potapenko<sup>b</sup>, W. Westmeier<sup>c</sup>, R. Brandt<sup>c</sup>

<sup>a</sup> School of Physics, University of Sydney, NSW 2006, Australia

<sup>b</sup> Joint Institute of Power and Nuclear Research-Sosny NASB, 220109 Minsk, Belarus

<sup>c</sup> Fachbereich Chemie, Philipps University, Marburg, Germany

### ARTICLE INFO

#### Article history:

Received 18 August 2011

Received in revised form

13 March 2012

Accepted 26 March 2012

Available online 2 April 2012

#### Keywords:

Fission residues

Spallation residues

Evaporation residues

Mica track detectors

### ABSTRACT

Detection of fission and spallation–evaporation residues resulting from interaction of relativistic protons with uranium, lead and gold targets in mica track detectors is investigated by the Monte Carlo method and using experimental data available in literature. It is shown that the contribution of spallation–evaporation residues to total track density is strongly dependent on target thickness and is the least for thick targets. This contribution in the case of thick target materials with  $Z \geq 79$  is less than or is within the statistical uncertainty of a typical track density measurement. Although our results on registration and detection of the spallation residues in mica are based on the interactions of uranium and lead with protons at 1A GeV and gold with protons at 0.8A GeV, they are applicable to all targets with  $Z \geq 79$  and for proton energies much higher than 1 GeV.

© 2012 Elsevier B.V. All rights reserved.

### 1. Introduction

Interaction of relativistic protons ( $E_p$  larger than a few hundred MeV) with heavy target nuclei results in emission of many product particles and ions. During the first stage of interaction the incident proton interacts with individual nucleons in the target nucleus, initiating a cascade of nucleon–nucleon collisions. This stage of the interaction is referred to as the intranuclear cascade (INC) and results in emission of nucleons, pions and some light ion from the target nucleus. The post-INC excited residual nuclei de-excite by evaporating light particles and/or fission. The reaction residues produced in the interaction will be referred to as fission residues if they have fission origin and spallation–evaporation residues if they have non-fission origin. Combination of all of these interaction stages together is referred to as spallation reaction.

We divide spallation–evaporation residues into two groups of light spallation–evaporation residues (LSER) and heavy spallation–evaporation residues (HSER). LSER mainly refer to light particles emitted during the INC stage of the interaction and post-INC evaporated particles. In general the HSER would be the partners of the LSER if excited nuclei de-excite via binary decay.

Track detectors [1] have been widely used to record tracks of charged nuclear particles and the products of spallation reaction is no exception. These detectors are used in studies related to

mechanisms and kinematics of spallation reactions as well as in determination of reaction cross-sections at different projectile energies and different target materials [2–7]. Mica is one of the commonly used track detectors. Mica track detectors are also used to record tracks of fission events induced by different projectiles to obtain the fission rate in different target materials [8–10].

In studies relating to spallation reactions the registered tracks (e.g. in mica) can have two origins; they are either due to spallation–evaporation residues or due to fission fragments. It is essential to know which group of reaction residues are recorded and to what extent. This is the aim of the work described in this paper.

In this paper we present and discuss the detection of reaction products in interaction of protons with different target materials using a mica detector. We will concentrate on three target materials: uranium, lead and gold, for which detailed experimental results are available in literature.

### 2. Monte Carlo calculations

#### 2.1. Energy spectra of spallation residues

Monte Carlo calculations were performed using the MCNPX 2.7a code [11], with the INCL4 intranuclear cascade model [12] and the ABLA fission-evaporation model [13] options. We investigated interactions of protons with target foils of U, Pb and Au. Calculations were performed for thin and thick target foils.

\* Corresponding author. Tel.: +61 2 93515964.

E-mail address: reza@physics.usyd.edu.au (S.R. Hashemi-Nezhad).

In this work we refer to a target as a thick target if

1. its thickness  $d$  is larger than the range of reaction products  $R$  in the target material;
2. the thickness  $d$  is much less than inelastic interaction mean free path of the incident ions in the target ( $d \ll \lambda_{in}$ ) and thus the flux of the projectile ions does not decay noticeably via inelastic interactions within the target;
3. the thickness  $d$  is much less than the range of incident ions in target material and thus energy loss of incident ions by means of electronic interactions is negligible.

The definition of thin target may vary from experiment to experiment and in this work we impose only one restriction and that is  $d < R$ . In this paper a foil of thickness  $30 \mu\text{m}$  will be referred to as a thick target.

Fig. 1a shows the calculated energy spectra of ions ( $Z > 2$ ) within the volume of thick targets of  $^{238}\text{U}$ ,  $^{208}\text{Pb}$  and  $^{197}\text{Au}$  when they have been irradiated with 1 GeV protons.

Fig. 1b shows the energy spectra of the ions that leak out of thick target foils. In Figs. 1 and 2 and other energy spectra shown in this paper, energy bins have a width of 0.5 MeV.

Fig. 2 shows the energy spectra of residue ions within the volume of a thick natural uranium foil irradiated with protons of energy 1, 1.5 and 5 GeV. Calculations were also performed for 10 GeV protons but the corresponding spectrum is not shown in Fig. 2 to maintain the clarity and simplicity of the figure.

Fig. 3 shows the energy spectra of the ions produced in interaction of 1 GeV protons with thick and thin ( $d = 0.5 \mu\text{m}$ )  $^{\text{nat}}\text{U}$  targets. The ion spectra within the target volume and spectra of the ions that leak out of the target foils are presented.

From Figs. 1–3 we make the following observations:

1. Obviously the spectra shown in Figs. 1–3 are affected by energy loss of fragments within the target material. This is quite obvious in Fig. 3, where ion spectra for two different target thicknesses are presented.
2. The energy spectra of the residue ions do not change significantly with the increasing proton energy from 1 to 10 GeV as can be seen in Fig. 2 for energies up to 5 GeV. In the cases of 1 and 1.5 GeV protons the ion energy spectra are almost identical; however spectra corresponding to 5 and 10 GeV protons are slightly different. Table 1 gives the fluences of the ions for energies less than and greater than 29 MeV as well as the total fluence. At  $\sim 29$  MeV the fluence of the ions at different incident proton energies is about the same and thus

this energy is used as a reference point. From Table 1 it can be seen that the ion fluence integrated over all energies is almost constant within the statistical uncertainties of the calculations ( $< 2\%$ ). At energies less than 29 MeV the ion fluence slightly increases with increasing proton energy. This increase is 3% for 5 GeV and 8% for 10 GeV protons as compared with the case of  $E_p = 1$  GeV.

From Fig. 2 and Table 1 we see that any conclusion obtained on the registration of reaction products in mica at proton energy of  $\sim 1$  GeV is applicable to proton energies up to 10 GeV with quite good accuracy.

3. The spectra of spallation–evaporation residues within the volume of target foils (Figs. 1 and 3) extend to energies above 150 MeV especially in the cases of 5 and 10 GeV protons; however their total fluence does not exceed 0.2% of the total ion fluence.
4. From Fig. 3 it is evident that spectra of residue ions within the target volume, as well as the leakage ions, are very different for the cases of thick and thin targets. As tracks in mica are produced by the ions that leak out of the target foil, the spectra shown in Fig. 3b are more relevant to our studies in this paper.

We calculated the ion spectra both for  $^{\text{nat}}\text{U}$  and  $^{238}\text{U}$  targets at different incident proton energies and obtained identical results,

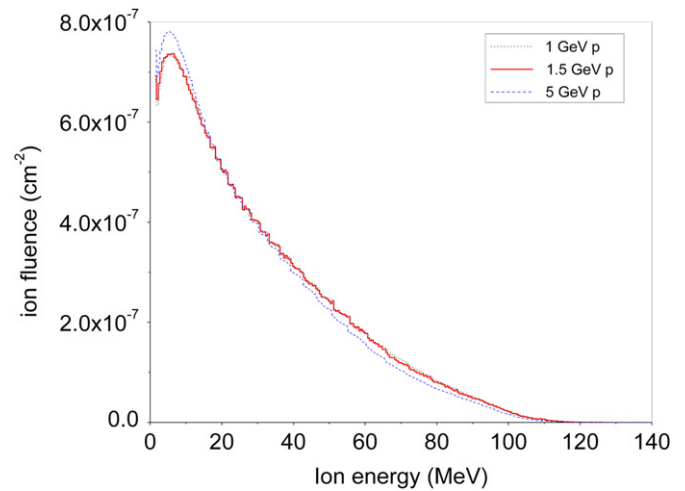


Fig. 2. Calculated spectra of the ions resulting from the interaction of proton of the energy 1, 1.5 and 5 GeV with natural uranium foil of thickness  $30 \mu\text{m}$  within the target volume.

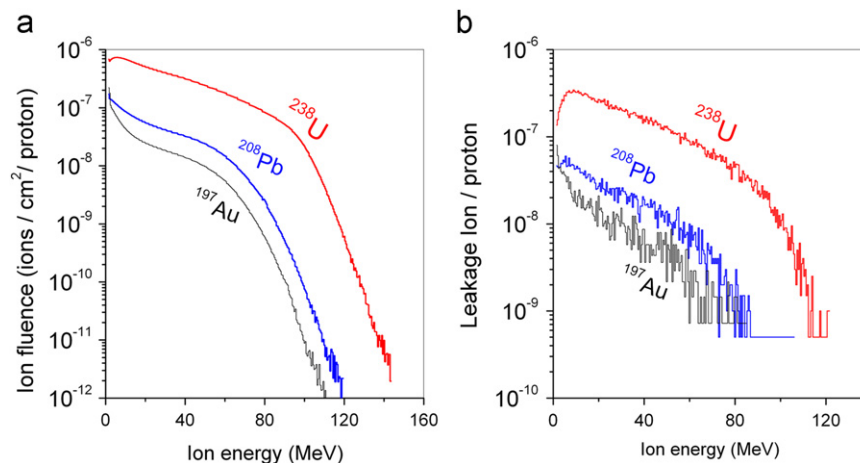
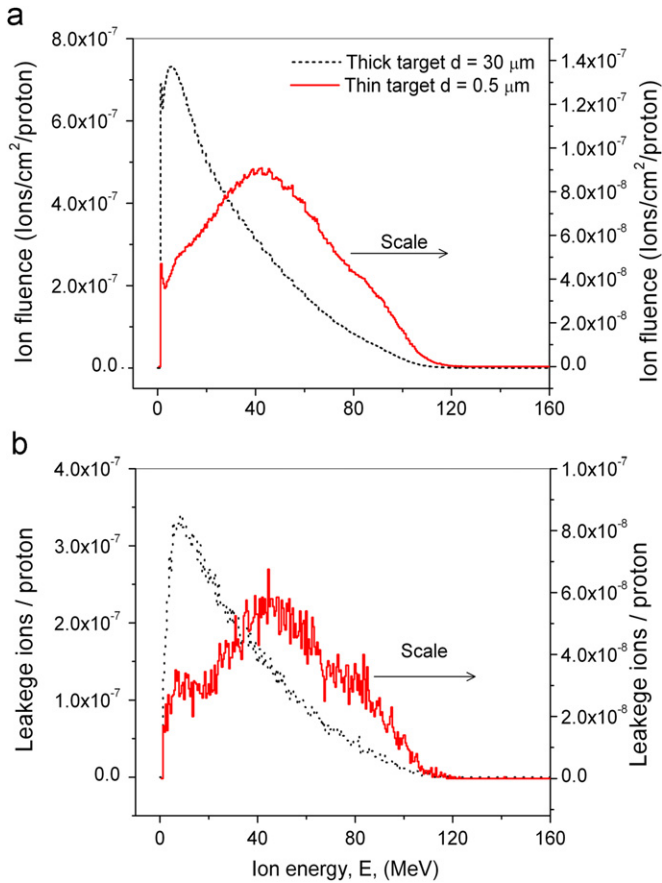


Fig. 1. Calculated energy spectra of ions with  $Z > 2$  when thick target foils of  $^{238}\text{U}$ ,  $^{208}\text{Pb}$  and  $^{197}\text{Au}$  were irradiated with 1 GeV protons. (a) Energy spectra of the ions within the volume of the target foils and (b) the energy spectra of the ions that leak out of thick target foils.



**Fig. 3.** Calculated spectra of the ions produced in interaction of 1 GeV protons with thick ( $d=30\ \mu\text{m}$ ) and thin ( $d=0.5\ \mu\text{m}$ ) uranium targets. (a) Ions energy distribution within the volume of the target and (b) ions that leak out of the target.

**Table 1**

Fluence of residues in the volume of a thick natural uranium target, per incident proton.

Proton energy (GeV)	$\varphi_{(E < 29)}\ (\text{cm}^{-2})$	$\varphi_{(E > 29)}\ (\text{cm}^{-2})$	$\varphi_{\text{total}}\ (\text{cm}^{-2})$
1	$3.26\text{E}-5$	$2.49\text{E}-05$	$5.75\text{E}-5$
1.5	$3.27\text{E}-5$	$2.46\text{E}-05$	$5.73\text{E}-5$
5	$3.36\text{E}-5$	$2.33\text{E}-05$	$5.69\text{E}-5$
10	$3.52\text{E}-5$	$2.21\text{E}-05$	$5.73\text{E}-5$

suggesting that presence of about 0.7%  $^{235}\text{U}$  in  $^{\text{nat}}\text{U}$  does not affect the energy spectra of the product nuclei.

## 2.2. Mass and charge of the residues

Fig. 4 shows the mass and charge distributions of reaction residues in interaction of 1.5 GeV protons with  $^{\text{nat}}\text{U}$ ,  $^{\text{nat}}\text{Pb}$  and  $^{197}\text{Au}$  targets of thickness  $30\ \mu\text{m}$ , calculated using the MCNPX code. For each distribution:

- The central peak is due to the fission residues.
- The data points beyond the minimum at the right-hand side of the fission peaks (e.g. around  $Z \sim 70$  for uranium target) are mainly due to HSER. This is supported by the experimental observations reported in [14–17].
- Light ions at the left-hand side of the fission peak are mainly due to the LSER [18] (not all particles are shown in the plots).

From Fig. 4 it is evident that there are charge and mass regions over which charge and mass distributions of the spallation–evaporation and fission residues overlap. This is more pronounced for the case of heavy residues.

## 3. Tracks of spallation–evaporation residues in mica

### 3.1. Registration threshold of mica detectors

Fleischer et al. [19] have shown that muscovite mica can register tracks of  $^{20}\text{Ne}$  at an energy of  $\sim 2\ \text{MeV}$ . Katcoff and Hudis [20] have set the detection threshold of mica at  $Z > 14$  and  $E > 8\ \text{MeV}$  while Khan [5] has used a charge threshold of  $Z=16$  for muscovite mica. It is also shown that  $^{20}\text{Ne}$  ions of energy  $\sim 2\ \text{MeV}$  could produce detectable tracks in biotite mica under suitable etching and observation conditions [21]. Therefore we conclude that the track registration threshold of mica is  $Z \geq 10$ .

### 3.2. Track detection threshold

For tracks that can be revealed by chemical etching, there is a minimum detectable track size. Obviously such a track size limitation is strongly dependent on the means of observation and detection. The track size limit in this paper refers to track analysis using an optical microscope with human operator (for details see Ref. [22]).

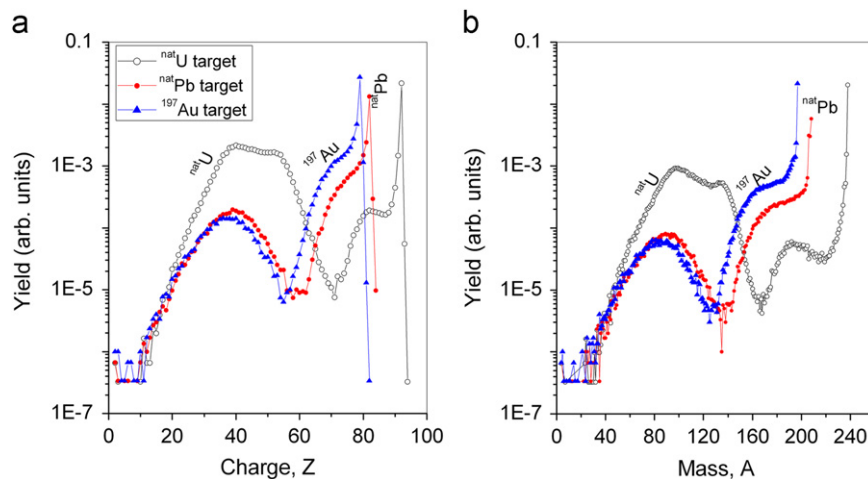


**Fig. 4.** Calculated charge and mass distribution of reaction residues in interactions of 1.5 GeV protons with thick targets of natural uranium, natural lead and gold.

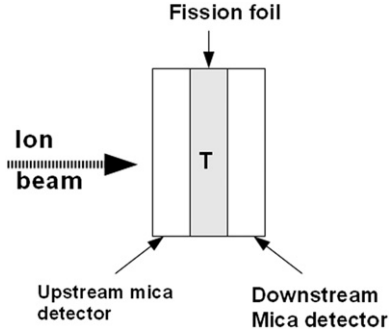


Fig. 5. Target-detector arrangement for the irradiations.

It is shown that in the case of mica a track depth limit of  $\delta = 1.63 \mu\text{m}$  is a suitable choice for detection threshold [22].

Moreover, in track detectors a charged particle track can be revealed by chemical etching only if dip angle of the track with respect to the detector surface is larger than a critical angle  $\theta_c$ . For mica  $\theta_c = 4.5^\circ$  [22].

### 3.3. Track densities due to fission and spallation–evaporation residues

The usual experimental setup is to prepare a sandwich of mica and target material as shown in Fig. 5. The target material (e.g. foil) is placed in close contact between two mica foils. The mica detectors are referred to as downstream and upstream detectors as shown in Fig. 5. The target material (T in Fig. 5) could be thin or thick. The sandwich is then placed in the particle field of interest (e.g. proton beam from an accelerator) for a given period of time. The interaction of incident particles with target nuclei results in production of energetic ions, some of which register in the mica as tracks. The irradiated mica detectors are then etched in suitable etching conditions, the etched tracks are examined under an optical microscope and the track densities are determined [22]. In this paper we will mainly consider the artificial mica (Fluorophlogopite) as the track detector, for which we have obtained a calibration factor for fission-rate determination and have used it extensively in our earlier experiments [8,10].

The track density in a track detector in close contact with a thick or thin target foil of thickness  $d$  is given by the following equations [22,23]:

$$\rho = \frac{n}{4} R \varepsilon N_v \sigma F, \quad \text{thick target; } d > R \quad (1)$$

$$\rho = \frac{n}{2} \left(1 - \frac{d}{2R}\right) d \varepsilon N_v \sigma F, \quad \text{thin target; } d < R \quad (2)$$

where  $n$  is number of fragments emitted per reaction of interest,  $d$  is thickness of target foil,  $R$  is range of fragments in the target material,  $\varepsilon$  is an efficiency factor which includes the critical angle effect [1] as well as the limitations imposed by the minimum detectable track size and track observation conditions,  $N_v$  is atom density of target foil,  $\sigma$  is reaction cross-section which is a constant for the case of irradiations with mono-energetic particles (protons) and  $F$  is time integrated incident particle fluence.

## 4. Registration and detection of spallation–evaporation residues

The excited nuclei, left over from the intranuclear cascade stage of the reaction, decay by emission of low  $Z$  nuclei in the process of de-excitation. The charge range of these nuclei is target type dependent and may vary with the incident particle type and energy.

As the charge detection threshold of mica is relevant to light reaction residues only, we study the registerability of light and heavy spallation–evaporation residues separately.

### 4.1. Light spallation–evaporation residues

Fig. 6 shows the calculated charge distribution of the interaction residues that escape thick foils of U, Pb and Au on their irradiation with 1 GeV protons. Similar to Fig. 4 the central peaks are due to the fission fragments. From Fig. 6 it is evident that almost all of the LSER (peaks at the left-hand side of the fission peak) have charges  $Z < 16$  (the ion charge threshold used in Ref. [5]). The LSER predominantly have charges less than 10. These ions defiantly will not register in mica as etchable tracks.

Fig. 6 shows that, some of the ions in the range of  $Z = 10–16$  are due to fission fragments. As already mentioned in Section 3.1 the registration threshold of the mica is in the range of  $Z = 10–16$  [5,19–21]. From Fig. 6 the residues with charge in the range of 10–16 are 0.5%, 3.7% and 7% of the fission fragments for U, Pb and Au targets, respectively. Therefore we conclude that the contribution of the LSER to total track density in the mica detectors will be insignificant.

### 4.2. Heavy spallation–evaporation residues

In this section we discuss the contribution of HSER to the recorded tracks in mica for three target materials, viz U, Pb and

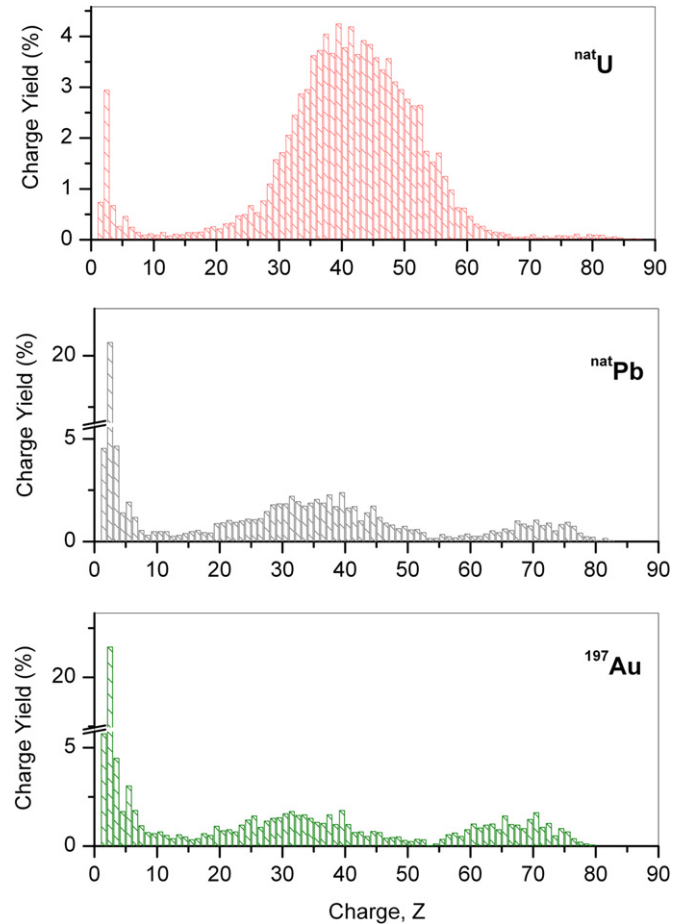
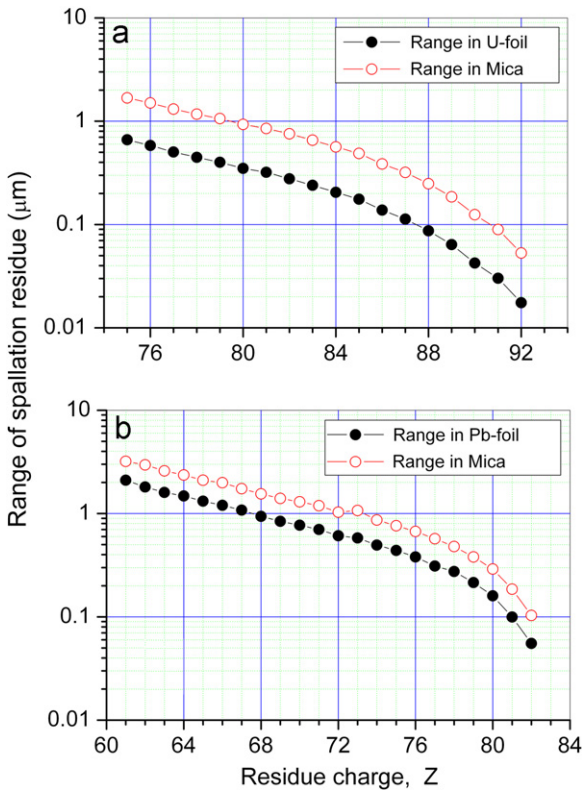


Fig. 6. Calculated charge distributions of the ions (fission fragments and spallation–evaporation residues) that escape the thick target foils of Au, Pb and U on their irradiation with protons of 1 GeV. The charge yields are given as percentages of total ions produced in a given interaction.

Au. Using Eq. (1) the ratio of track densities due to fission to that of the spallation–evaporation residues for a thick target is given by

$$\frac{\rho_f}{\rho_s} = 2 \frac{R_f \sigma_f \varepsilon_f}{R_s \sigma_s \varepsilon_s} \quad (3)$$

where the subscripts  $f$  and  $s$  refer to fission fragments and heavy spallation–evaporation residues, respectively. In obtaining Eq. (3) we have assumed that all fission events are binary; thus  $n_f=2$ . In the case of heavy spallation–evaporation residues  $n_s=1$  was used (only heavy spallation–evaporation residues will register if track registration conditions as given in Sections 3.1 and 3.2 are satisfied) and it was assumed that emission direction of the spallation–evaporation residues does not depend on their mass as reported in Refs. [2] and references therein. It is expected that the mean registration–detection–efficiency for fission fragments to be larger than that for the spallation–evaporation residues i.e.  $(\varepsilon_f/\varepsilon_s) \geq 1$ .



**Fig. 7.** Range of heavy spallation residues in the target material and the mica detector. (a) HSER ( $Z=75\text{--}92$ ) from  $^{238}\text{U}$  (1AGeV)+p reaction, data from Ref. [25]. (b) HSER ( $Z=61\text{--}82$ ) from Pb (1AGeV)+p reaction, data from Ref. [26]. Range calculations were performed using the SRIM code.

**Table 2**

Parameters used to calculate the ratio of track density due to fission to track density due to HSER. The  $\rho_f/\rho_s$  values represent the lower limits. The cross-section values refer to U+p and Pb+p at 1A GeV and Au+p at 0.8A GeV. For the thin target  $d=0.5\ \mu\text{m}$  was used. For details of ion range estimations refer to the text. For each target thickness, the contribution of the HSER to total track density  $\rho_t=\rho_f+\rho_s$  is given in percentages.

Target	$\sigma_f$ (mb)	$\sigma_s$ (mb)	$R_f$ ( $\mu\text{m}$ )	$R_s$ ( $\mu\text{m}$ )	Thick foil		Thin foil		Very thin foil	
					$\rho_f/\rho_s$	$\rho_s/\rho_t$ (%)	$\rho_f/\rho_s$	$\rho_s/\rho_t$ (%)	$\rho_f/\rho_s$	$\rho_s/\rho_t$ (%)
U	1530	10	4.75	0.7	2076	0.05	450	0.22	306	0.33
Pb	157	25.27	7.84	2	49	2.00	14	6.67	12	7.69
Au	74.2	25.77	4.44	1	26	3.57	7	12.50	6	14.29

For a target which is thin for both fission fragments and HSER (i.e.  $d < R_f$  and  $d < R_s$ ), from Eq. (2) we have

$$\frac{\rho_f}{\rho_s} = 2 \frac{(1-d/2R_f) \sigma_f \varepsilon_f}{(1-d/2R_s) \sigma_s \varepsilon_s} \quad (4)$$

For the case of  $d \ll R$  ( $R_f$  and  $R_s$ ) Eq. (4) becomes

$$\frac{\rho_f}{\rho_s} \approx 2 \frac{\sigma_f \varepsilon_f}{\sigma_s \varepsilon_s} \quad (5)$$

We calculated the  $\rho_f/\rho_s$  for thick and thin targets of U, Pb and Au as described below.

#### 4.2.1. Uranium target

In interaction of  $^{238}\text{U}$  and proton at 1A GeV the fission fragments of  $Z=28\text{--}74$  have kinetic energies in the range of 92.2 – 16.7 MeV [14,15]. The mean fission fragment has  $\langle Z \rangle = 44.9 \pm 0.1$  and mean kinetic energy  $\langle E_K \rangle = 76 \pm 3$  MeV and the most probable fragment is  $^{107}\text{Rh}$  [14]. Thus the range of the mean fission fragment of uranium in metallic uranium foil is  $R_f=4.75\ \mu\text{m}$  [24].

Mean kinetic energies of heavy HSER in the interaction of  $^{238}\text{U}$  and proton at 1A GeV in the charge range of  $Z=75\text{--}92$  occupy the energy range of 8.34–0.19 MeV [25]. The range of these HSER in U-foil and mica are shown in Fig. 7a. Maximum ranges of these residues (corresponding to range of 8.34 MeV Re) in U-foil and mica are 0.7  $\mu\text{m}$  and 1.68  $\mu\text{m}$ , respectively.

The total reaction cross-section for the interaction of  $^{238}\text{U}$  with protons at 1A GeV is  $1.99 \pm 0.17$  b of which  $\sigma_f=1.53 \pm 0.13$  b is due to fission process [14]. From Fig. 14 of [18] and cross-section data given in Ref. [16] it is evident that total cross-section for the production of HSER that may result in detectable tracks cannot exceed 10 mb. Using these data and Eqs. (3)–(5), the ratios of the track density due to fission to track density due to the spallation–evaporation residues ( $\rho_f/\rho_s$ ) were calculated as given in Table 2. For the thin target  $d=0.5\ \mu\text{m}$  was used.

#### 4.2.2. Lead target

In interaction of protons with lead at 1A GeV the HSER have masses in the range of  $A=141\text{--}207$ . The weighted mean kinetic energies of HSER are in the range of 9.67–0.09 MeV [26]. In this interaction the highest kinetic energy of the HSER is 11.12 MeV corresponding to Pm isotopes ( $Z=61$ ) and kinetic energy of the residues decreases with increasing charge number to 0.45 MeV at  $Z=82$  [26].

The range of the HSER in metallic lead (the target material) is in the range of 0.06–2  $\mu\text{m}$  as shown in Fig. 7b. Thus only HSER produced within a layer of thickness  $\sim 2\ \mu\text{m}$  of Pb-foil can contribute to the tracks in the detector.

Ranges of full-energy HSER in mica extend from 0.1 to 3.2  $\mu\text{m}$  and calculations show that only HSER ions with  $Z \leq 67$  can result in tracks with the sizes above the detection threshold of the mica detector ( $\delta=1.63\ \mu\text{m}$  [22]).

In the Pb+p reaction at 1A GeV the mean kinetic energy of single fission fragments is in the range of  $34.1 \pm 2.2$  MeV for  $Z=58$  and  $67.4 \pm 1.1$  MeV for  $Z=22$ . Using  $\langle E_K \rangle = 64$  MeV as the

mean kinetic energy of single fission fragment and  $\langle Z \rangle \approx 40$  and  $\langle A \rangle \approx 91$  as the mean charge and mean mass number of the mean fission fragment [26] one obtains a mean range of  $R_f = 7.84 \mu\text{m}$ . For HSER we use  $R_s = 2 \mu\text{m}$  corresponding to the most energetic heavy spallation–evaporation residue. The fission cross-section for Pb+p at 1A GeV reaction is  $\sigma_f = 157 \pm 26 \text{ mb}$  [26] and for HSER we use  $\langle \sigma_s \rangle = 25.27 \text{ mb}$  as the cross-section for the production of HSER with  $Z \leq 67$  [26]. Using these data the track density ratios ( $\rho_f/\rho_s$ ) were calculated as given in Table 2.

#### 4.2.3. Gold target

For the gold target we used the experimental results given in Ref. [27] to obtain an estimate of  $(\rho_f/\rho_s)_{\text{Au}}$ . In the reaction of 0.8A GeV Au with protons, Z number of fission fragments predominantly is in the range of 20–60, with the fissioning nucleus being  $Z=75$  and  $A=170$  and the mean total kinetic energy of fission fragments is  $114 \pm 2 \text{ MeV}$  [28]. In this reaction the mean fission fragment has  $\langle A \rangle \approx 85$  and  $\langle Z \rangle \approx 37$ . We used  $\langle E_k \rangle = 57 \text{ MeV}$  as mean kinetic energy of the gold fission fragments. This mean fission fragment has a range of  $R_f = 4.44 \mu\text{m}$  in the gold foil.

The average kinetic energies of HSER are  $0 < \langle E_k \rangle \leq 9 \text{ MeV}$ , with  $Z=60$  being the lowest Z-value of the HSER [27]. From the charge and  $\langle E_k \rangle$  values given in Fig 10 of Ref. [27] it becomes clear that all HSER have ranges less than  $0.95 \mu\text{m}$  in Au. This implies that the mean range of HSER in gold foil is much less than  $1 \mu\text{m}$ . Thus negligibly small number of HSER could escape Au-foil and those that do escape will have dramatically degraded kinetic energy and therefore their ranges in mica will be much less than the detection threshold of  $\delta = 1.63 \mu\text{m}$ .

For an extreme case we assume that all HSER enter the mica with their energy undegraded. Then from Z-numbers and kinetic energies of the ions [27] it becomes clear that only residues with Z in the range of 60–66 can have ranges larger than the detection threshold. Total production cross-section for fragments in this charge range is  $25.77 \text{ mb}$  [27]. For fission cross-section of (0.8A GeV Au+p) the value  $\sigma_f = 74.2 \text{ mb}$  from Ref. [29] was used which is in agreement with the experimental findings of Ref. [28]. These data were used to calculate the track density ratios for thick and thin gold targets as shown in Table 2.

It should be noted that the track density ratios ( $\rho_f/\rho_s$ ) and  $(\rho_s/\rho_t)$  given in Table 2 are the lowest and highest limits, respectively, because

1. In Eqs. (3)–(5),  $\varepsilon_f/\varepsilon_s = 1$  was used, while it is expected that  $\varepsilon_f > \varepsilon_s$ .
2. In the case of the Au target the range of the HSER in mica was highly overestimated with the hypothetical assumption that the HSER enter the mica detector without losing energy within the gold foil.

## 5. Discussion and conclusions

Monte Carlo calculations of the interaction of protons with the target materials ( $Z \geq 79$ ) show that the overall energy spectrum of the residue ions does not change significantly with increasing energy of the protons (example of uranium target illustrated in Fig. 2).

It is shown experimentally that in interactions of protons with thick gold targets the mean kinetic energy of a given residue (spallation–evaporation and fission residue) either decreases or remains almost constant with increasing projectile proton energy over the energy range of 1–300 GeV [2]. This is true for light fragments (e.g.  $^{24}\text{Na}$ ), medium mass nuclides (e.g.  $^{54}\text{Mn}$ ), neutron excess nuclei (e.g.  $^{103}\text{Ru}$ ) and neutron deficient nuclei (e.g.  $^{131}\text{Ba}$ ).

In the case of medium mass nuclei such as  $^{87}\text{Y}$  the kinetic energy is reduced by a factor of two when the incident proton energy increases from 1 to 11.5 GeV [2]. The latter may imply that charges and masses of the post-INC fissioning exited nuclei have decreased significantly with increasing incident proton energy from 1 to 11.5 GeV and thus, the kinetic energies of fission fragments are reduced [30].

A measure of the mean ranges of the fragments in the interaction of protons of different energies with uranium shows that mean range of the light products such as  $^{24}\text{Na}$  increases to a maximum at  $\sim 3 \text{ GeV}$  and then decreases with increasing energy of the incident protons [2,4]. Such an increase is  $\sim 20\%$  when the proton energy is increased from 0.7 to 3 GeV. However this effect is not that obvious in the case of the gold target. Such a range increase of LSER will not affect the conclusions of this paper because majority of LSER will not be registered due to the existence of charge threshold for registration of tracks in mica.

Thus although in the present paper the detectability of the reaction residues are based on U+p and Pb+p at 1A GeV and Au+p at 0.8A GeV, the conclusions remain valid for higher proton energies.

It is shown that on exposure of a mica detector to spallation–evaporation products resulting from interaction of relativistic protons with metallic targets with  $Z \geq 79$  the contributions of the tracks due to light and heavy spallation–evaporation residues to total track density in the mica detectors (cf. Fig. 6 and Table 2) are negligible.

In general, the contribution of HSER to total track density in mica ( $\rho_t = \rho_f + \rho_s$ ) is the lowest for the case of *thick targets* (Table 2). For this type of target the HSER share of total track density is less than or within the typical statistical uncertainties of track density measurements. The highest contribution of HSER is in the case of very thin targets. Therefore it is obvious that for the type of experiments in which the number of fission events has prime importance, such as the case of fission rate measurements, thick targets must be used.

Although results obtained and discussed in this work are based on three target types, uranium, lead and gold, they can be generalised to all target types with  $Z \geq 79$ . This is because of the fact that the ratio  $\rho_f/\rho_s$  strongly depends on the cross-section ratio  $\sigma_f/\sigma_s$  which increases with increasing Z-number of the target element.

## Acknowledgments

The Authors would like to thank Dr. K-H. Schmidt of GSI for providing the data for kinetic energies of the heavy spallation residues in interaction of  $^{238}\text{U}$  and proton at 1A GeV (Ref. [25]).

## References

- [1] R.L. Fleischer, P.B. Price, R.M. Walker, Nuclear Tracks in Solids, University of California Press, 1975.
- [2] S.B. Kaufman, E.P. Steinberg, M.W. Weisfield, Physical Review C 18 (1978) 1349.
- [3] S.B. Kaufman, E.P. Steinberg, B.D. Wilkins, Physical Review Letters 41 (1978) 1359.
- [4] S.B. Kaufman, M.W. Weisfield, Physical Review C 11 (1975) 1258.
- [5] H.A. Khan, Journal of Physics G: Nuclear Physics 14 (1988) 701.
- [6] M. Debeauvais, J. Tripier, S. Jokic, Z. Todorovic, R. Antanasijevic, Physical Review C 23 (1981) 1624.
- [7] G. Rémy, J. Ralarosy, R. Stein, M. Debeauvais, J. Tripier, Nuclear Physics A 163 (1971) 583.
- [8] S.R. Hashemi-Nezhad, I. Zhuk, M. Kievets, M.I. Krivopustov, A.N. Sosnin, W. Westmeier, R. Brandt, Nuclear Instruments and Methods in Physics Research Section A 591 (2008) 517.
- [9] S.R. Hashemi-Nezhad, I. Zhuk, A. Potapenko, M. Kievets, M.I. Krivopustov, Nuclear Instruments and Methods in Physics Research A 664 (2012) 154.

- [10] J.J. Borger, S.R. Hashemi-Nezhad, D. Alexiev, R. Brandt, W. Westmeier, B. Thomauske, J. Adam, M. Kadykov, S. Tyutyunnikov, *Nuclear Instruments and Methods in Physics Research A* 664 (2012) 103.
- [11] D.B. Pelowitz, J.S. Hendricks, J.W. Durkee, M.R. James, M.L. Fensin, G.W. McKinney, S.G. Mashnik, and L.S. Waters, MCNPX 2.7.A Extensions, Report LA-UR-08-07182, Los Alamos National Laboratory, November 6, 2008.
- [12] A. Boudard, J. Cugnon, S. Leray, C. Volant, *Physical Review C* 66 (2002) 044615.
- [13] A.R. Junghans, M. d. Jong, H.-G. Clerc, A.V. Ignatyuk, G.A. Kadyaev, K.-H. Schmidt, *Nuclear Physics A* (1998) 635.
- [14] M. Bernas, P. Armbruster, J. Benlliure, A. Boudard, E. Casarejos, S. Czajkowski, T. Enqvist, R. Legrain, S. Leray, B. Mustapha, P. Napolitani, J. Pereira, F. Rejmund, M.-V. Ricciardi, K.-H. Schmidt, C. Stéphan, J. Taieb, L. Tassan-Got, C. Volant, *Nuclear Physics A* 725 (2003) 213.
- [15] M. Bernas, P. Armbruster, J. Benlliure, A. Boudard, E. Casarejos, T. Enqvist, A. Kelic, R. Legrain, S. Leray, J. Pereira, F. Rejmund, M.-V. Ricciardi, K.-H. Schmidt, C. Stéphan, J. Taieb, L. Tassan-Got, C. Volant, *Nuclear Physics A* 765 (2006) 197.
- [16] J. Taieb, K.-H. Schmidt, L. Tassan-Got, P. Armbruster, J. Benlliure, M. Bernas, A. Boudard, E. Casarejos, S. Czajkowski, T. Enqvist, R. Legrain, S. Leray, B. Mustapha, M. Pravikoff, F. Rejmund, C. Stéphan, C. Volant, W. Wlazlo, *Nuclear Physics A* 724 (2003) 413.
- [17] P. Armbruster, J. Benlliure, M. Bernas, A. Boudard, E. Casarejos, S. Czajkowski, T. Enqvist, S. Leray, P. Napolitani, J. Pereira, F. Rejmund, M.-V. Ricciardi, K.-H. Schmidt, C. Stéphan, J. Taieb, L. Tassan-Got, C. Volant, *Physical Review Letters* 93 (2004) 212701.
- [18] M.V. Ricciardi, P. Armbruster, J. Benlliure, M. Bernas, A. Boudard, S. Czajkowski, T. Enqvist, A. Kelic, S. Leray, R. Legrain, B. Mustapha, J. Pereira, F. Rejmund, K.-H. Schmidt, C. Stéphan, L. Tassan-Got, C. Volant, O. Yordanov, *Physical Review C* 73 (2006) 014607.
- [19] R.L. Fleischer, B.P. Price, R.M. Walker, E.L. Hubbard, *Physical Review* 156 (1967) 353.
- [20] S. Katcoff, J. Hudis, *Physical Review Letters* 28 (1972) 1066.
- [21] S.R. Hashemi-Nezhad, S.A. Durrani, *Nuclear Tracks* 5 (1981) 189.
- [22] S.R. Hashemi-Nezhad, I. Zhuk, A.S. Potapenko, M.I. Krivopustov, *Nuclear Instruments and Methods in Physics Research Section A* 568 (2006) 816.
- [23] A.P. Malykhin, O.I. Yaroshevich, V.A. Levadni, L.P. Roginetc, *Vestsi AS BSSR Ser. Phys.-Energ. Navuk* 2 (1970) 16.
- [24] J.F. Ziegler, J.P. Biersack, U. Littmark, *The Stopping and Range of Ions in Matter*, Pergamon Press, 1985 See also <www.SRIM.org>.
- [25] K.-H. Schmidt, GSI, Private communications, email: K.H.Schmidt@gsi.de 2009.
- [26] T. Enqvist, W. Wlazlo, P. Armbruster, J. Benlliure, M. Bernas, A. Boudard, S. Czajkowski, R. Legrain, S. Leray, B. Mustapha, M. Pravikoff, F. Rejmund, K.-H. Schmidt, C. Stéphan, J. Taieb, L. Tassan-Got, C. Volant, *Nuclear Physics A* 686 (2001) 481.
- [27] F. Rejmund, B. Mustapha, P. Armbruster, J. Benlliure, M. Bernas, A. Boudard, J.P. Dufour, T. Enqvist, R. Legrain, S. Leray, K.-H. Schmidt, C. Stéphan, J. Taieb, L. Tassan-Got, C. Volant, *Nuclear Physics A* 683 (2001) 540.
- [28] J. Benlliure, P. Armbruster, M. Bernas, A. Boudard, J.P. Dufour, T. Enqvist, R. Legrain, S. Leray, B. Mustapha, F. Rejmund, K.-H. Schmidt, C. Stéphan, L. Tassan-Got, C. Volant, *Nuclear Physics A* 683 (2001) 513.
- [29] A.V. Prokofiev, *Nuclear Instruments and Methods in Physics Research A* 463 (2001) 557.
- [30] V.E. Viola, K. Kwiatkowski, M. Walker, *Physical Review C* 31 (1985) 1550.